RSC Advances

PAPER

View Article Online
View Journal | View Issue

Cite this: *RSC Adv.*, 2020, **10**, 15734

Photocurrent generation by a photosystem I-NiO photocathode for a p-type biophotovoltaic tandem cell†

Yuya Takekuma,[a] Nobuhiro Ikeda,[a] Keisuke Kawakami,[b] Nobuo Kamiya,[c] Mamoru Nango[c] and Morio Nagata *[a]

Received 25th February 2020
Accepted 15th April 2020

DOI: 10.1039/d0ra01793k

rsc.li/rsc-advances

Photosynthesis is a process used by algae and plants to convert light energy into chemical energy. Due to their uniquely natural and environmentally friendly nature, photosynthetic proteins have attracted attention for use in a variety of artificial applications. Among the various types, biophotovoltaics based on dye-sensitized solar cells have been demonstrated in many studies. Although most related works have used n-type semiconductors, a p-type semiconductor is also a significant potential component for tandem cells. In this work, we used mesoporous NiO as a p-type semiconductor substrate for Photosystem I (PSI) and demonstrated a p-type PSI-biophotovoltaic and tandem cell based on dye-sensitized solar cells. Under visible light illumination, the PSI-adsorbed NiO electrode generated a cathodic photocurrent. The p-type biophotovoltaic cell using the PSI-adsorbed NiO electrode generated electricity, and the IPCE spectrum was consistent with the absorption spectrum of PSI. These results indicate that the PSI-adsorbed NiO electrode acts as a photocathode. Moreover, a tandem cell consisting of the PSI-NiO photocathode and a PSI-TiO_2 photoanode showed a high open-circuit voltage of over 0.7 V under illumination to the TiO_2 side. Thus, the tandem strategy can be utilized for biophotovoltaics, and the use of other biomaterials that match the solar spectrum will lead to further progress in photovoltaic performance.

Introduction

Photosynthesis is a process used by algae and plants to convert light energy into chemical energy. In order to reduce the consumption of fossil fuels and curb global warming, the efficient use of sunlight by mimicking photosynthesis or directly using photosynthetic proteins is attracting attention. Photosynthetic proteins, which use highly complex and optimized processes that are impossible to reproduce, have been reportedly used in a variety of artificial applications such as biophotovoltaics, semi-artificial photosynthesis, biosensors, biosupercapacitors, and photosynthetic microbial fuel cells.[1–7] As biomaterials, various photosynthetic protein-pigment complexes such as photosystem I (PSI), photosystem II (PSII), reaction centers/light-harvesting antenna complexes (RC-LH1), light-harvesting complexes (LHCII), *etc.* have been researched for artificial utilization. These biomaterials are naturally abundant and pose no threat to the environment. In addition, the reaction center of a protein-pigment complex exhibits near-unity quantum efficiency attributable to spatial charge separation by multiple sequential electron-transfer pathways within the protein, which is a very attractive feature for researchers in the photoenergy-conversion field.

Generally, these biomaterials have been deposited onto various electrodes such as gold, graphene, and metal-oxide semiconductors to create photocathodes and photoanodes.[8] These electrodes are used alone or in a combination of two electrodes.[9–13] As one application, biophotovoltaics have been demonstrated using these biohybrid electrodes.[1,14] Especially, biophotovoltaics based on dye-sensitized solar cells (DSSCs)[15] have been investigated using the metal-oxide semiconductors, TiO_2, Fe_2O_3 and ZnO as the electrode.[14,16–22] DSSCs generally consist of a dye-sensitized photoanode, Pt counter electrode, and electrolyte. In 2012, Mershin *et al.* reported PSI-based DSSCs on nanostructured TiO_2 and ZnO electrodes using a Co(II/III) redox mediator.[16] Similarly, Kondo *et al.* demonstrated PSI- and PSII-based DSSCs using a TiO_2 electrode,[17] and in 2015, Yu *et al.* achieved the most effective PSI- and LHCII-based DSSC to date using two different particle sizes of TiO_2.[18] Furthermore, polyaniline/TiO_2 (ref. 19) and hematite semiconductor electrodes[20] have also been investigated as

[a]*Department of Industrial Chemistry, Graduate School of Engineering, Tokyo University of Science, 12-1 Ichigaya-funagawara, Shinjuku-ku, Tokyo 162-0826, Japan. E-mail: nagata@ci.tus.ac.jp*

[b]*Research Center for Artificial Photosynthesis (ReCAP), Osaka City University, 3-3-138 Sugimoto, Sumiyoshi-ku, Osaka 558-8585, Japan*

[c]*The OCU Advanced Research Institute for Natural Science & Technology (OCARINA), Osaka City University, 3-3-138 Sugimoto, Sumiyoshi-ku, Osaka 558-8585, Japan*

† Electronic supplementary information (ESI) available. See DOI: 10.1039/d0ra01793k

photoanodes for biophotovoltaic-based DSSCs. Although most studies have used n-type metal-oxide semiconductors as the photoanode, a p-type semiconductor would also be significant because it could be used as the photocathode component in a tandem cell.[23,24] The tandem cell has attracted interest because high photovoltaic performances can be achieved by simply replacing a Pt counter electrode with a photocathode. In biophotovoltaics, a tandem cell is also an effective strategy for increasing the photoresponse and improving the photovoltaic performance.[25] For example, Ravi *et al.* developed a biohybrid tandem cell consisting of two stacked sub-cells connected in parallel,[25] which led to photocurrent enhancement by complementary absorption of the two RC-LH1 units.

Here, we used mesoporous NiO as a p-type semiconductor substrate for PSI and demonstrated PSI-biophotovoltaics based on p-type DSSCs and a tandem cell. The NiO electrode has often been used for p-type DSSCs.[24,26,27] The power conversion mechanism of p-type DSSCs begin with excitation of the dye, after which the hole is transferred from the dye to the valence band of the semiconductor, while the electron reduces the redox agent in the electrolyte; this is the reverse direction compared with n-type DSSCs. In PSI, upon photoexcitation of the chlorophyll dimer, called P700, the excited electron on P700 is transferred to the primary electron acceptor Chl *a* (A_0, Fig. 1), the secondary acceptor phylloquinone (A_1), and finally the acceptor [4Fe–4S] iron–sulfur clusters (F_X, F_A, and F_B).[28] This multi-step, sequential, unidirectional electron transfer has a near unity charge-separation quantum efficiency.[28,29] We fabricated a PSI-adsorbed NiO electrode and biophotovoltaics based on p-type DSSCs and confirmed that the PSI-adsorbed NiO electrode acts as the photocathode. Moreover, a tandem biophotovoltaic cell was demonstrated consisting of the PSI-NiO photocathode and the well-known photoanode PSI-TiO_2. Our fabricated tandem cell exhibited an open-circuit voltage of over 0.7 V, which is comparable to that of other biophotovoltaics exhibiting high photovoltages.[30,31]

Results & discussion

PSI-adsorbed NiO electrode

Mesoporous NiO-coated FTO glass was fabricated based on a previous method[32] with slight modifications. A scanning electron microscope (SEM) image of the NiO electrode is shown in Fig. S1.† The SEM image shows that there are 50–500 nm NiO particles, which form larger pores than the PSI trimer diameter (*ca.* 21 nm). These results indicate that PSI can enter the NiO pores.

For deposition onto the NiO electrode, PSI core complexes were purified from *Thermosynechococcus vulcanus* according to previous methods[33–35] with slight modifications. PSI was then deposited onto the NiO electrode by a vacuum-assisted drop-casting method.[36] To confirm the presence of PSI, the UV-visible spectrum of the PSI-adsorbed NiO electrode was measured and is shown Fig. S2.† In the UV-visible spectrum, two distinct peaks at 680 nm and 440 nm are present corresponding to the Q-band and Soret-band absorption of chlorophyll in PSI, respectively, which indicated the presence of PSI on the NiO electrode. In addition, the amount of adsorbed PSI was calculated to be 4.55 ± 0.42 μgChl cm^{-2} by measuring the absorption of chlorophyll desorbed from the NiO electrode using an acetone solution. This value is larger than the adsorbable amount of PSI on a 1 cm^2 plane (calculated as 0.097 μgChl). Collectively, these results indicate that PSI was adsorbed not only onto the NiO surface but also inside the mesopores of the NiO film, as shown in Fig. 1.

Electrochemical and photoelectrochemical experiments

The electrochemical properties and photocurrent response of the PSI-adsorbed NiO electrode were investigated. These experiments employed a Pt counter electrode and Ag/AgCl (saturated KCl) reference electrode in an aqueous solution containing 0.1 M phosphate buffer (pH 7) and 0.1 M $NaClO_4$. The cyclic voltammograms of NiO electrodes with and without PSI are shown in Fig. 2a. The bare NiO electrode exhibited a quasi-reversible electrochemistry and distinct peaks in both the anodic and cathodic scans. These peaks are attributable to the redox reaction of surface Ni.[37] Upon scanning the cathode, the surface Ni^{II} first oxidizes to Ni^{III} and then to Ni^{IV}. In the PSI-adsorbed NiO electrode, these peaks decreased. In addition, the cyclic voltammogram indicated a slower oxidation reaction than that of the bare NiO electrode, and there appeared to be a peak shift toward a higher potential. These results indicate that PSI was adsorbed onto the NiO surface.

Fig. 2b shows the photocurrent response of the NiO electrodes with and without PSI. The photocurrent at 0 mV *vs.* Ag/AgCl was measured under illumination by a Xe lamp with a 420 nm long-pass filter to exclude the photocurrent of NiO. In the PSI-NiO electrode, a cathodic photocurrent of −0.75 ± 0.01 μA cm^{-2} occurred, whereas the photocurrent from NiO was hardly observed. The electron flow can be explained as follows: the excited electron at P700 on the luminal side transfers to the stromal side and is then used to oxidize the electron acceptor (in this case, oxygen), while the oxidized P700 receives an electron from the NiO surface (Fig. 1b). The charge on the NiO surface is transported to the FTO through the NiO/electrolyte interface,[38] and consequently, a photocurrent is generated. Moreover, addition of the well-known electron acceptor methyl viologen (MV^{2+}) increase the cathodic photocurrent of PSI to

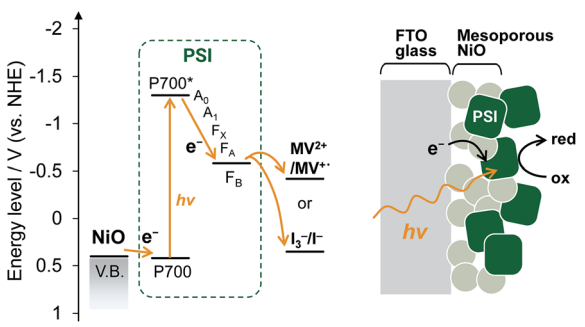

Fig. 1 Energy levels and schematic representation of the PSI-adsorbed NiO photocathode.

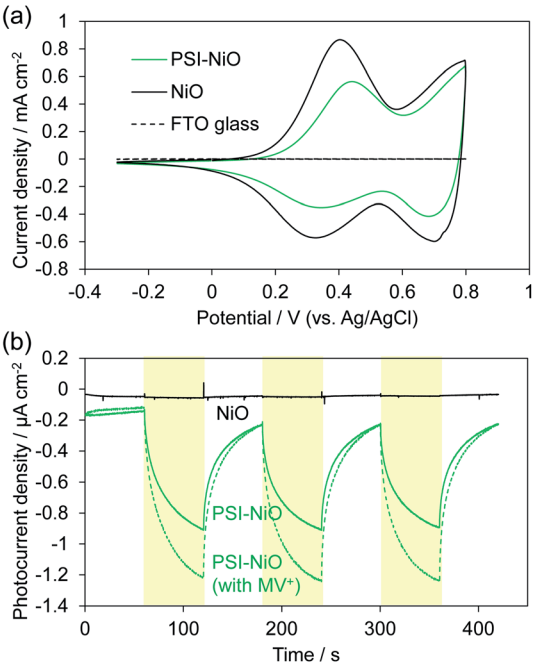

Fig. 2 (a) Cyclic voltammograms of NiO (black) and PSI-NiO (green) electrodes in the dark in a 0.1 M phosphate aqueous buffer (pH 7) solution. The potential of the working electrode was scanned from −0.3 to 0.8 V *vs.* Ag/AgCl at a rate of 50 mV s^{-1}. (b) Photoelectrochemical measurements of NiO (black), PSI-NiO without methyl viologen (MV^{2+}) (green solid), and PSI-NiO with MV^{2+} (green dash) at 0 mV *vs.* Ag/AgCl in a 0.1 M phosphate aqueous buffer (pH 7) solution containing 0.1 M $NaClO_4$. The experiment was performed under AM 1.5G illumination with a 420 nm long-pass filter. The intensity was *ca.* 85 mW cm^{-2}.

-1.10 ± 0.09 μA cm^{-2}. This is because the reaction rate of MV^{2+} with PSI is higher than that with oxygen.[39] For comparison, when using the n-type semiconductor TiO_2, the resulting photocurrent is anodic.[21,40] Overall, these results indicate that the PSI-NiO electrode acts as a photocathode. In addition, the photocurrent response at various potentials was also measured, and the results are shown Fig. S3.† At −200 mV *vs.* Ag/AgCl, a cathodic photocurrent also occurred, whereas at +300 mV *vs.* Ag/AgCl, an anodic photocurrent occurred. In this case, the electron flow begins with an excited electron on P700 transferring to NiO, after which the oxidized P700 receives an electron from the electron donor in the electrolyte. Therefore, the results indicate that PSI was adsorbed in different orientations on the NiO surface.

Photovoltaic characteristics

Biophotovoltaics based on p-type DSSCs were fabricated using the PSI-NiO photocathode. To investigate the photovoltaic performances of the p-type biophotovoltaics, a two-electrode sandwich cell was prepared with the PSI-NiO electrode, a Pt counter electrode, and a triiodide/iodide-based ionic liquid electrolyte according to a previous report.[41] Table 1 and Fig. 3 show the photovoltaic performances under 1 sun conditions (AM 1.5G) and the IPCE spectrum, respectively. Our fabricated

Table 1 Average photocurrent density–voltage (*J*–*V*) characteristics of biophotovoltaic cells using PSI-NiO electrodes and PSI-TiO_2 and tandem cell under AM 1.5G (100 mW cm^{-2}) and their respective standard deviations (7 biophotovoltaic cells)

	J_{SC}/mA cm^{-2}	V_{OC}/V	FF	PCE/%
PSI-NiO	0.16 ± 0.01	0.10 ± 0.01	0.42 ± 0.01	0.0071 ± 0.0003
Tandem cell	0.16 ± 0.01	0.71 ± 0.01	0.50 ± 0.02	0.056 ± 0.001
PSI-TiO_2	0.15 ± 0.01	0.58 ± 0.02	0.59 ± 0.03	0.053 ± 0.008

p-type biophotovoltaic exhibited a 0.16 ± 0.01 mA cm^{-2} short-circuit current density (J_{SC}), a 0.10 ± 0.01 V open-circuit voltage (V_{OC}), and a 0.0071 ± 0.0003% power conversion efficiency (PCE). The IPCE spectrum of the p-type biophotovoltaic is consistent with the distinct absorption peak at 680 nm, as shown Fig. 3. These results show that PSI acts as a photosensitizer in the biophotovoltaic based on p-type DSSCs.

To investigate whether the PSI-NiO photocathode could be used in a tandem cell, we demonstrated a PSI-based tandem cell consisting of a PSI-NiO photocathode and PSI-TiO_2 photoanode in a simple sandwich configuration according to Fig. 4a. When light was incident to the tandem cell, the PSI adsorbed onto NiO reduces the redox agent, and an electron is received from NiO. On the other hand, the PSI adsorbed onto TiO_2 receives an electron from the redox agent and injects it into TiO_2, resulting in current flow. For comparison, PSI-sensitized solar cells each using a PSI-NiO electrode or PSI-TiO_2 electrode were also demonstrated. The PSI-TiO_2 electrode and photovoltaic were fabricated according to previously reported procedures.[41] In the photovoltaic measurement, the light was illuminated on the TiO_2 side, and the thickness of the top film was optimized to allow incident light on the bottom electrode (NiO film: 9 μm, TiO_2 film: 3 μm). The amounts of PSI adsorbed onto the electrodes were calculated as 6.01 ± 0.30 μgChl cm^{-2} (NiO electrode) and 6.27 ± 0.15 μgChl cm^{-2} (TiO_2 electrode). The series connection of the photoanode and photocathode in the tandem cell showed that the photocurrent is governed by the weakest photoelectrode, whereas the photovoltages are additive. Indeed, the photocurrent of the tandem cell was 0.16 ± 0.01 mA cm^{-2}, which is similar to that of the PSI-TiO_2 cell, whereas the V_{OC} of

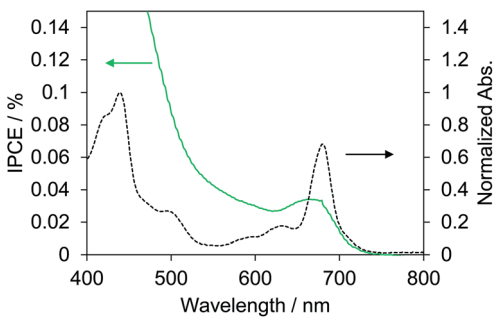

Fig. 3 IPCE spectrum of the best biophotovoltaic cell using the PSI-NiO electrode (green solid) and normalized absorption spectrum of PSI in HEPES buffer (black dash). Absorbance is normalized against the maximum peak.

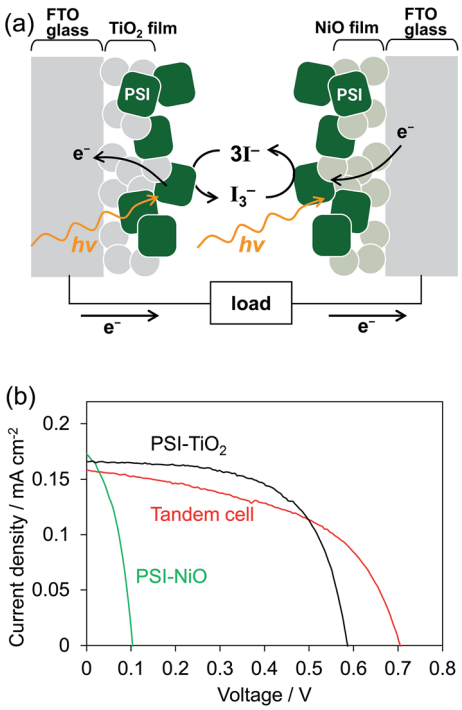

Fig. 4 (a) Schematic representation of the tandem cell power generation mechanism. (b) J–V curves under AM 1.5G (100 mW cm^{-2}) of the tandem cell and individual n- and p-biophotovoltaic cells.

the tandem cell matched the sum of the V_{OC} values of the PSI-TiO_2 and PSI-NiO cells, as shown in Fig. 4b. Consequently, the V_{OC} was improved to 0.71 ± 0.01 V, and the PCE was 0.056 ± 0.001%. This V_{OC} is comparable to that of other bio-photovoltaics that have exhibited high photovoltages.[30,31] However, the fill factor (FF) of the tandem cell was lower than that of PSI-TiO_2. This is due to the low shunt resistance of the tandem cell, which might be attributable to shade from the top cell and/or increased recombination at the semiconductor/electrolyte interface.[42,43] In summary, our fabricated PSI-NiO photocathode was utilized in a tandem cell that exhibited a high voltage when irradiated on the TiO_2 side. However, the photocurrent was low because the same bio-sensitizer was used for the photocathode and photoanode. Thus the use of other biomaterials that match the solar spectrum will be required to further increase the photovoltaic performance.

Conclusion

In summary, we fabricated a PSI-adsorbed NiO electrode for utilization as a component in a tandem cell and demonstrated p-type biophotovoltaics based on DSSCs using the PSI-NiO electrode. Under visible light illumination, the electrode showed a cathodic photocurrent, and the photovoltaic was powered by PSI, which indicates that the PSI-NiO electrode acts as a photocathode. Moreover, we demonstrated a tandem cell consisting of the PSI-NiO photocathode and a PSI-TiO_2 photoanode. The tandem cell exhibited a high V_{OC} of over 0.7 V under illumination on the TiO_2 side.

Tandem cells have the advantages of a simple fabrication method employed by changing the Pt counter electrode and a high V_{OC} since it does not depend on the redox potential of the redox agents but instead on the conduction band minimum of the photoanode and valence band maximum of the photocathode. Therefore, selection of appropriate redox agents could lead to more efficient photovoltaic performances. Moreover, controlling the PSI orientation to match the current flow and using other photosynthetic proteins that can absorb a broad spectral region could also lead to further improvements to the efficiency of these biophotovoltaics.

Experiments

Materials

All chemicals were purchased from commercial suppliers and used without purification.

Purification of PSI of *T. vulcanus*[33–35,41]

Harvested *T. vulcanus* cells were treated with lysozyme for 90 min at 38 °C in darkness, then centrifuged at 10 000*g* for 10 min. The obtained precipitants were suspended with a small amount of buffer containing 25% (w/v) glycerol, 20 mM HEPES–NaOH (pH 7.0), and 10 mM $MgCl_2$. Subsequently, the samples were stored at −80 °C, and the thylakoid membranes were obtained by a freeze-thawing method.[44] The thylakoid membranes were solubilized with 0.6% (w/v) *n*-dodecyl-β-D-maltoside (β-DDM), then centrifuged at 38 900*g* for 90 min at 4 °C. Subsequently, the obtained supernatants were filtrated through a 0.45 μm filter and loaded onto an anion-exchange column (DEAE TOYOPEARL 650S) with 5% (w/v) glycerol, 30 mM Mes (pH 6.0), 3 mM $CaCl_2$, and 0.03% (w/v) β-DDM. The column was washed with the same buffer containing 80 mM NaCl to remove the large amount of phycobilisome impurities. Elution of the PSI core complexes was carried out with a linear gradient from 80 to 140 mM NaCl in the same buffer.

Fabrication of electrodes for photoelectrochemical measurements

The NiO pastes consisted of 18 wt% NiO nanoparticles, 9 wt% ethyl cellulose (EC), and 73 wt% terpineol. Two kinds of EC powders, EC (Kanto Kagaku, 10cP) and EC (Kanto Kagaku, 45cP) (65/35, v/v), were dissolved in ethanol. The ethanolic mixtures were added to a round-bottom flask containing NiO nanopowder (Sigma-Aldrich, <50 nm particle size) and terpineol. This mixture was then ultrasonicated for 48 h, and the ethanol was removed by rotary-evaporator. Finally, the pastes were made with a three-roll mill (EXAKT, Nagase Screen Printing Research). The nanocrystalline NiO paste was coated onto fluorine-doped SnO_2 (FTO) conductive glass plates (Nippon Sheet Glass) by squeegee for photoelectrochemical measurements, and the electrodes were sintered at 450 °C for 30 min and then 550 °C for 15 min in air. PSI was deposited onto the NiO electrode according to the vacuum-assisted drop-casting method reported Faulkner *et al.*;[36] an aqueous solution of PSI (*ca.* 0.4 mgChl mL^{-1}) containing 0.1 M HEPES buffer was dropped onto the

NiO electrode, and the electrode was placed under vacuum for 120 min. Subsequently, the electrode was rinsed with water and dried with N_2 gas.

Electrochemical and photoelectrochemical measurements

All measurements were performed using a potentiostat (HSV-110, Hokuto Denko) with a Pt counter electrode and Ag/AgCl (saturated KCl) reference electrode in an aqueous solution containing phosphate buffer (0.1 M, pH 7) and 0.1 M $NaClO_4$. For the cyclic voltammetry measurements, the potential of the working electrode was scanned from −0.3 to 0.8 V *vs.* Ag/AgCl at a rate of 50 mV s^{-1}. Photochronoamperometric measurements were performed with a Xe lamp solar simulator (XB-500E, Peccell Technologies) and a 420 nm long-pass filter with using an illumination time of 60 s (*ca.* 85 mW cm^{-2}). The light intensity was measured by Si solar cell (BS-520, Bunkokeiki) placed in front of the electrochemical cell. MV^{2+} was employed as an electron donor at 3 mM.

Fabrication of biophotovoltaics

The FTO glass was coated with a 0.05 M nickel acetate ethanol solution by dip-coating and subsequently dried at room temperature before screen printing. The NiO photocathode was screen-printed using the above-mentioned NiO paste, and the electrodes were sintered at 450 °C for 30 min and then at 550 °C for 15 min in air. PSI was adsorbed onto the NiO electrode by immersion in a PSI buffer solution (*ca.* 0.4 mgChl mL^{-1}). The photovoltaic device was fabricated by sandwiching a 30 μm Surlyn spacer between the stained NiO photocathode and a Pt counter electrode. The electrolyte solution was introduced into the cell *via* a predrilled hole in the Pt counter electrode. The electrolyte consisted of 0.2 M I_2 and 0.1 M guanidine thiocyanate in 1-ethyl-3-methylimidazolium tricyanomethanide and 1-methyl-3-propylimidazolium iodide (13 : 7 v/v). The tandem cell was fabricated in the same manner but with the PSI-TiO_2 photoanode instead of the Pt counter electrode. The TiO_2 photoanode was fabricated by screen-printing, and the thickness was optimized to allow light incident to the bottom NiO electrode.

Characterization of bio-photovoltaic devices

The photovoltaic performances of the fabricated solar cells were evaluated by the incident photon-to-current conversion efficiency (IPCE) spectra and photocurrent density–voltage (*J–V*) measurements. The IPCE spectra were measured with a Peccell Technologies S10AC system and the *J–V* curves were measured under AM 1.5G one-sun conditions (100 mW cm^{-2}) with a Yamashita Denso YSS-150A. The light intensity was calibrated with reference to a Si solar cell (BS-520, Bunkokeiki)

Conflicts of interest

There are no conflicts to declare.

Acknowledgements

Y. Takekuma and M. Nagata would like to thank Mr Masaki Saito (Department of Industrial Chemistry, Tokyo University of Science, Japan) for measuring a scanning electron microscope image. M. Nango thanks for the support of the Grant, AOARD (Grant No. FA2386-19-1-4033).

Notes and references

1 S. K. Ravi, V. S. Udayagiri, L. Suresh and S. C. Tan, *Adv. Funct. Mater.*, 2018, **28**, 1705305.
2 N. Kornienko, J. Z. Zhang, K. K. Sakimoto, P. Yang and E. Reisner, *Nat. Nanotechnol.*, 2018, **13**, 890–899.
3 A. J. McCormick, P. Bombelli, R. W. Bradley, R. Thorne, T. Wenzel and C. J. Howe, *Energy Environ. Sci.*, 2015, **8**, 1092–1109.
4 A. Antonacci and V. Scognamiglio, *TrAC Trends Anal. Chem.*, 2019, **115**, 100–109.
5 L. Liu and S. Choi, *Biosens. Bioelectron.*, 2019, **140**, 111354.
6 M. Rosenbaum, Z. He and L. T. Angenent, *Curr. Opin. Biotechnol.*, 2010, **21**, 259–264.
7 M. Sawa, A. Fantuzzi, P. Bombelli, C. J. Howe, K. Hellgardt and P. J. Nixon, *Nat. Commun.*, 2017, **8**, 1327.
8 K. Nguyen and B. D. Bruce, *Biochim. Biophys. Acta*, 2014, **1837**, 1553–1566.
9 T. Kothe, N. Plumeré, A. Badura, M. M. Nowaczyk, D. A. Guschin, M. Rögner and W. Schuhmann, *Angew. Chem., Int. Ed.*, 2013, **52**, 14233–14236.
10 V. Hartmann, T. Kothe, S. Pöller, E. El-Mohsnawy, M. M. Nowaczyk, N. Plumeré, W. Schuhmann and M. Rögner, *Phys. Chem. Chem. Phys.*, 2014, **16**, 11936–11941.
11 M. Rasmussen, A. Shrier and S. D. Minteer, *Phys. Chem. Chem. Phys.*, 2013, **15**, 9062–9065.
12 K. P. Sokol, W. E. Robinson, A. R. Oliveira, J. Warnan, M. M. Nowaczyk, A. Ruff, I. A. C. Pereira and E. Reisner, *J. Am. Chem. Soc.*, 2018, **140**, 16418–16422.
13 F. Zhao, P. Wang, A. Ruff, V. Hartmann, S. Zacarias, I. A. C. Pereira, M. M. Nowaczyk, M. Rögner, F. Conzuelo and W. Schuhmann, *Energy Environ. Sci.*, 2019, **12**, 3133–3143.
14 E. Musazade, R. Voloshin, N. Brady, J. Mondal, S. Atashova, S. K. Zharmukhamedov, I. Huseynova, S. Ramakrishna, M. M. Najafpour, J.-R. Shen, B. D. Bruce and S. I. Allakhverdiev, *J. Photochem. Photobiol., C*, 2018, **35**, 134–156.
15 B. O'Regan and M. Gratzel, *Nature*, 1991, **353**, 737–740.
16 A. Mershin, K. Matsumoto, L. Kaiser, D. Yu, M. Vaughn, M. K. Nazeeruddin, B. D. Bruce, M. Graetzel and S. Zhang, *Sci. Rep.*, 2012, **2**, 234.
17 M. Kondo, M. Amano, T. Joke, S. Ishigure, T. Noji, T. Dewa, Y. Amao and M. Nango, *Res. Chem. Intermed.*, 2014, **40**, 3287–3293.
18 D. Yu, M. Wang, G. Zhu, B. Ge, S. Liu and F. Huang, *Sci. Rep.*, 2015, **5**, 9375.
19 E. A. Gizzie, J. Scott Niezgoda, M. T. Robinson, A. G. Harris, G. Kane Jennings, S. J. Rosenthal and D. E. Cliffel, *Energy Environ. Sci.*, 2015, **8**, 3572–3576.

20 K. Ocakoglu, T. Krupnik, B. van den Bosch, E. Harputlu, M. P. Gullo, J. D. J. Olmos, S. Yildirimcan, R. K. Gupta, F. Yakuphanoglu, A. Barbieri, J. N. H. Reek and J. Kargul, *Adv. Funct. Mater.*, 2014, **24**, 7467–7477.
21 V. B. Shah, W. R. Henson, T. S. Chadha, G. Lakin, H. Liu, R. E. Blankenship and P. Biswas, *Langmuir*, 2015, **31**, 1675–1682.
22 M. Nagata, M. Amano, T. Joke, K. Fujii, A. Okuda, M. Kondo, S. Ishigure, T. Dewa, K. Iida, F. Secundo, Y. Amao, H. Hashimoto and M. Nango, *ACS Macro Lett.*, 2012, **1**, 296–299.
23 J. He, H. Lindström, A. Hagfeldt and S.-E. Lindquist, *Sol. Energy Mater. Sol. Cells*, 2000, **62**, 265–273.
24 A. Nattestad, A. J. Mozer, M. K. R. Fischer, Y. B. Cheng, A. Mishra, P. Bäuerle and U. Bach, *Nat. Mater.*, 2010, **9**, 31–35.
25 S. K. Ravi, Z. Yu, D. J. K. Swainsbury, J. Ouyang, M. R. Jones and S. C. Tan, *Adv. Energy Mater.*, 2017, **7**, 1601821.
26 I. R. Perera, T. Daeneke, S. Makuta, Z. Yu, Y. Tachibana, A. Mishra, P. Bäuerle, C. A. Ohlin, U. Bach and L. Spiccia, *Angew. Chem., Int. Ed.*, 2015, **54**, 3758–3762.
27 F. Odobel, Y. Pellegrin, E. A. Gibson, A. Hagfeldt, A. L. Smeigh and L. Hammarström, *Coord. Chem. Rev.*, 2012, **256**, 2414–2423.
28 N. Nelson and C. F. Yocum, *Annu. Rev. Plant Biol.*, 2006, **57**, 521–565.
29 S. W. Hogewoning, E. Wientjes, P. Douwstra, G. Trouwborst, W. van Ieperen, R. Croce and J. Harbinson, *Plant Cell*, 2012, **24**, 1921–1935.
30 P. I. Gordiichuk, G.-J. A. H. Wetzelaer, D. Rimmerman, A. Gruszka, J. W. de Vries, M. Saller, D. A. Gautier, S. Catarci, D. Pesce, S. Richter, P. W. M. Blom and A. Herrmann, *Adv. Mater.*, 2014, **26**, 4863–4869.
31 V. K. Singh, S. K. Ravi, J. W. Ho, J. K. C. Wong, M. R. Jones and S. C. Tan, *Adv. Funct. Mater.*, 2018, **28**, 1703689.
32 S. Ito, T. N. Murakami, P. Comte, P. Liska, C. Grätzel, M. K. Nazeeruddin and M. Grätzel, *Thin Solid Films*, 2008, **516**, 4613–4619.
33 J.-R. Shen and N. Kamiya, *Biochemistry*, 2000, **39**, 14739–14744.
34 K. Kawakami, M. Iwai, M. Ikeuchi, N. Kamiya and J.-R. Shen, *FEBS Lett.*, 2007, **581**, 4983–4987.
35 J.-R. Shen, K. Kawakami and H. Koike, in *Photosynthesis Research Protocols*, ed. R. Carpentier, Humana Press, Totowa, NJ, 2011, pp. 41–51, DOI: 10.1007/978-1-60761-925-3_5.
36 C. J. Faulkner, S. Lees, P. N. Ciesielski, D. E. Cliffel and G. K. Jennings, *Langmuir*, 2008, **24**, 8409–8412.
37 G. Boschloo and A. Hagfeldt, *J. Phys. Chem. B*, 2001, **105**, 3039–3044.
38 H. Zhu, A. Hagfeldt and G. Boschloo, *J. Phys. Chem. C*, 2007, **111**, 17455–17458.
39 G. E. Milanovsky, A. A. Petrova, D. A. Cherepanov and A. Y. Semenov, *Photosynth. Res.*, 2017, **133**, 185–199.
40 V. V. Nikandrov, Y. V. Borisova, E. A. Bocharov, M. A. Usachev, G. V. Nizova, V. A. Nadtochenko, E. P. Lukashev, B. V. Trubitsin, A. N. Tikhonov, V. N. Kurashov, M. D. Mamedov and A. Y. Semenov, *High Energy Chem.*, 2012, **46**, 200–205.
41 Y. Takekuma, H. Nagakawa, T. Noji, K. Kawakami, R. Furukawa, M. Nango, N. Kamiya and M. Nagata, *ACS Appl. Energy Mater.*, 2019, **2**, 3986–3990.
42 S. Chen, J. Weng, Y. Huang, C. Zhang, L. Hu, F. Kong, L. Wang and S. Dai, *J. Phys. D: Appl. Phys.*, 2010, **43**, 305102.
43 H. Choi, T. Hwang, S. Lee, S. Nam, J. Kang, B. Lee and B. Park, *J. Power Sources*, 2015, **274**, 937–942.
44 R. Nagao, A. Ishii, O. Tada, T. Suzuki, N. Dohmae, A. Okumura, M. Iwai, T. Takahashi, Y. Kashino and I. Enami, *Biochim. Biophys. Acta, Bioenerg.*, 2007, **1767**, 1353–1362.